International Journal of Technology

http://ijtech.eng.ui.ac.id

Research Article

Investigation of Graphene Oxide Synthesized from Recycled Battery Waste as a Friction Modifier in Polyalphaolefin Lubricants

Alfian Ferdiansyah Madsuha[1,2*], Timotius Tanusondjaja[1], Muhammad Ibadurrohman[3], Cahyo Setyo Wibowo[4], Riesta Anggarani[4], Havid Aqoma[5]

[1]Department of Metallurgical and Materials Engineering, Faculty of Engineering, Universitas Indonesia, Kampus Baru UI, Depok, 16424, Indonesia

[2]Tropical Renewable Energy Center (TREC), Faculty of Engineering, Universitas Indonesia, Kampus Baru UI, Depok, 16424, Indonesia

[3]Department of Chemical Engineering, Faculty of Engineering, Universitas Indonesia, Kampus Baru UI, Depok, 16424, Indonesia

[4]Department of Product Application Technology, Testing Centre for Oil and Gas LEMIGAS, 12230 South Jakarta, Indonesia

[5]Kelip-kelip!, Center of Excellence for Light Enabling Technologies, School of Energy and Chemical Engineering, Xiamen University Malaysia, Darul Ehsan, Selangor, 43900 Malaysia

*Corresponding author: alfian@eng.ui.ac.id; Tel.: +6221-786-3610

Abstract: This study investigates graphene oxide (GO) derived from recycled graphite in spent dry cell batteries as a friction modifier in polyalphaolefin (PAO)-based lubricants. GO was incorporated at weight fractions of 1, 3, and 5 wt% to evaluate its influence on friction reduction, wear mitigation, and lubrication film stability. The incorporation of GO significantly enhanced the tribological performance of PAO compared with that of the neat base oil. A nonlinear concentration-dependent relationship was observed between the coefficient of friction (CoF) and wear scar diameter (WSD). The 1 wt% GO–PAO formulation exhibited the lowest CoF, achieving approximately a 45% reduction relative to pure PAO, a 54% decrease in WSD, and a 9% improvement in lubricant film stability. This superior friction performance is attributed to the formation of a thin, well-dispersed tribofilm that effectively reduces interfacial shear stress under boundary lubrication conditions. In contrast, the minimum WSD was obtained at 3 wt% GO, displaying that the formation of a thicker or more compact protective layer enhanced the load-bearing capacity. Increasing the concentration to 5 wt% did not yield further improvement, likely due to reduced dispersion efficiency at higher loading levels. Overall, 1 wt% GO demonstrates optimal friction-reducing behavior, while moderate concentrations primarily contribute to enhanced wear resistance, highlighting a concentration-dependent friction–wear trade-off. These findings demonstrate a viable and sustainable pathway for upcycling battery waste into high-value lubricant additives, contributing to the development of multifunctional and environmentally friendly tribological systems.

Keywords: Battery waste; Friction Modifier; Graphene Oxide; Lubricant; Tribology

1. Introduction

Friction and wear are fundamental responses within tribological systems and are widely recognized as primary contributors to mechanical inefficiencies and material degradation in both automotive and industrial machinery (Abdelbary and Chang, 2023a; Abdelbary and Chang, 2023b; Kato, 2000). Friction dissipates mechanical energy in the form of heat, which reduces the moving components' energy transfer efficiency (Amiri and Khonsari, 2010). Approximately one-third of the total fuel energy consumed by passenger vehicles is lost to frictional dissipation

https://doi.org/10.14716/ijtech.v17i3.8377
Received January 2026; Revised February 2026; Accepted March 2026

within key components, such as the engine, transmission, tires, and braking systems (Holmberg et al., 2012). These adverse conditions escalate the maintenance requirements and shorten the critical components' operational lifespan (Wong and Tung, 2016). Hence, lubricants are crucial in mitigating these effects by forming a protective film that separates contacting surfaces, thereby reducing direct metal-to-metal interaction (Brinksmeier et al., 2015; Bowden et al., 1997).

Lubricants are developed in various physical states—liquid, solid, and gaseous—though oils and greases remain the most widely utilized in industrial and automotive applications (Li et al., 2022). Contemporary lubricant systems typically comprise base oils blended with specialized additives designed to enhance performance, thereby directly influencing tribological properties and functional stability. Conventional liquid lubricants may become ineffective under certain extreme operating conditions, such as those involving high loads, elevated temperatures, or vacuum environments, due to thermal degradation or loss of film integrity. Under such circumstances, solid lubricants are a viable alternative, offering superior load-bearing capacity, thermal stability, and failure resistance in boundary or dry lubrication regimes (Abdelbary and Chang, 2023a). Despite their advantages, the applicability of solid lubricants is constrained by their inherently finite film thickness, which gradually diminishes with continued use, ultimately reducing their long-term effectiveness (Erdemir and Donnet, 2001). Moreover, their tribological performance is susceptible to variations in the testing or operational environment, including surface roughness, temperature, and humidity. To overcome these limitations, recent advancements have focused on incorporating solid lubricants as additives within liquid lubricant formulations. This hybrid lubrication strategy harnesses the superior load-bearing capacity and thermal stability of solid lubricants while mitigating the limitations of conventional base oils. As a result, the synergistic interaction between solid additives and the liquid matrix enhances film formation, reduces friction, and improves wear resistance under demanding operating conditions. Consequently, lubrication technology advancements remain a pivotal focus of tribological research.

Carbon-based nanostructures have recently attracted considerable attention in tribology, particularly as high-performance additives in lubricants. Their unique structural, mechanical, and chemical properties enable them to effectively reduce friction, minimize wear, and extend the operational lifespan of mechanical components under diverse operating conditions(Opia et al., 2025; Wang et al., 2024; Nyholm and Espallargas, 2023). In this context, significant research efforts have focused on carbon-based nanomaterials—such as fullerenes, carbon nanotubes (CNTs), and carbon onions—as promising solid lubricant additives due to their superior physicochemical properties (Dai et al., 2024; Perreault et al., 2015). Among them, graphene oxide (GO) has emerged as a desirable candidate due to its favorable tribological properties, cost-effectiveness, and ease of production due to its scalable synthesis from abundant graphite using relatively simple chemical liquid-phase processes (Hummers and Offeman, 1958). Moreover, it has been reported that GO exhibits a strong affinity for metallic surfaces, especially steel, enabling rapid adsorption via hydrogen bonding or electrostatic interactions (Kozlov et al., 2012). This robust interfacial adhesion promotes the formation of a thin, conformal tribo-film on steel surfaces, analogous to the boundary layers established by conventional lubricants such as fatty acids. The protective film is an effective barrier against direct asperity contact, mitigating adhesive wear, and reducing friction in boundary lubrication regimes. Furthermore, under mechanical load, the intrinsic layered structure of GO facilitates interlaminar sliding between adjacent sheets, providing an additional mechanism for friction reduction and contributing to the lubrication system's overall stability (Kinoshita et al., 2015; Kinoshita et al., 2014; Liu et al., 2013).

One of the distinguishing characteristics of GO lies in the abundance of oxygen-containing functional groups—such as hydroxyl, carboxyl, and epoxy moieties—distributed across its basal planes and sheet edges. These polar functional groups endow GO with high surface activity and hydrophilicity, enhancing its dispersibility in polar solvents, particularly water. This improved colloidal stability facilitates its uniform incorporation into aqueous or other polar lubricant systems, ensuring consistent dispersion and effective interaction with the base fluid and contacting surfaces (Dreyer et al., 2010; Paredes et al., 2008). However, GO exhibits significant dispersion

challenges when dispersed in non-polar solvents, such as mineral oils and synthetic hydrocarbons, due to its intrinsically hydrophilic and polar surface. Consequently, surface functionalization is imperative for improving media compatibility. Recent studies have focused on tailoring the surface chemistry of GO by functionalizing it with long alkyl chains, nonionic surfactants, or grafting agents. These modifications increase the lipophilicity of GO, thereby enhancing its dispersion stability in non-polar base oils while maintaining its tribological efficacy and structural integrity under operational conditions (Kimura et al., 2025; Zapata-Hernandez et al., 2022; Son et al., 2021).

Conventional GO synthesis often relies on high-purity graphite derived from mined or synthetic sources, which presents sustainability and cost concerns. As industries move toward circular economy principles, interest in sourcing graphene precursors from waste materials, especially those rich in carbon, such as spent batteries and electronic waste, has increased. Battery primer waste—an underutilized by-product of primary battery manufacturing and disposal—contains significant residual graphite. This graphite, typically discarded in landfills, offers a viable carbon source for nanomaterial synthesis if properly purified and processed. Graphite flakes can be isolated and recovered from the waste matrix using physical separation and thermal treatment methods, providing an eco-friendly and low-cost precursor for GO production.

In recent years, biolubricants have emerged as a promising research trend in the tribology field (Gasni et al., 2017). The use of organic materials, polymers, and biomass-derived compounds as sustainable additives in lubricant formulations has been widely investigated (Pavani et al., 2017). In particular, GO has been widely synthesized either from commercially available graphite or from biomass-derived carbon precursors and subsequently applied as a friction-reducing additive in lubricant systems. However, to the best of our knowledge, no previous study has reported the use of graphite recovered from electronic waste—specifically battery primer waste—as a precursor for GO synthesis in tribological applications. In this study, GO synthesized from battery primer waste is incorporated as a friction modifier additive material for poly-alpha olefin (PAO), a widely used non-polar liquid oil base. From an engineering perspective, the challenge is twofold: (1) determining whether battery waste-derived GO can achieve comparable or superior friction- and wear-reduction performance relative to conventionally synthesized GO and (2) optimizing its concentration and dispersion stability in poly-alpha olefin (PAO). Therefore, this study addresses a critical engineering gap by systematically evaluating battery waste–derived GO as a friction modifier in PAO and optimizing its concentration to obtain excellent tribological performance. The tribological behavior is assessed using key performance indicators, including the coefficient of friction (CoF), tribofilm formation, and wear scar diameter (WSD), to identify the optimal loading that balances dispersion stability and interfacial protection.

This work establishes a technically viable pathway for upcycling battery primer waste into high-value functional nanomaterials beyond demonstrating friction and wear reduction. By integrating resource recovery with lubrication engineering optimization, this study advances sustainable materials utilization and high-performance tribological system design, contributing to the broader development of green manufacturing technologies.

2. Methods

The experimental methodology of this work consists of four main stages: GO preparation from battery waste, GO synthesis, GO functionalization, and subsequent characterization and tribological evaluation. This stepwise approach was designed to establish clear structural–property–performance relationships relevant to lubrication applications. Each experimental step is described in detail in the following subsections.

2.1 Graphite preparation from the battery waste

The process began with collecting spent dry cell batteries, which served as a source of graphite rods. Each battery was carefully dismantled to access the central graphite rod using cutting pliers. The extracted rods were manually cleaned to remove residual electrolyte and external contaminants. To eliminate any adhered manganese oxide (MnO_2) or other battery reaction by-products, the rods were thoroughly wiped and gently abraded using fine sandpaper. Once cleaned, the graphite rods were mechanically crushed into smaller fragments. The resulting powder was subsequently sieved using a 200-mesh stainless steel sieve to obtain fine graphite particles. This sieving step aimed to increase the specific surface area, facilitating more effective oxidation in the subsequent synthesis of graphene oxide.

2.2 Synthesis of Graphene Oxide (GO)

Graphene oxide was synthesized from graphite powder derived from spent dry cell batteries via a modified Hummers method (Zaaba et al., 2017; Hummers and Offeman, 1958). Initially, 3.0 g of graphite powder was introduced into a mixed acid solution containing concentrated H_2SO_4 (360 mL of concentrated H_2SO_4 and 40 mL of H_3PO_4 in a volumetric ratio of 9:1). The mixture was stirred at 330 rpm and room temperature (approximately 25°C) for 48 h to ensure adequate pre-oxidation and acid intercalation.

After 48 h of stirring, 9.0 g of $KMnO_4$ was slowly added to the reaction mixture while maintaining the temperature below 20 °C using an ice bath to avoid thermal runaway. Subsequently, the oxidation reaction was continued for an additional 24 h under continuous stirring. Subsequently, the reaction mixture was diluted with 200 mL of deionized water (aquadest or aquademine) and stirred for 5 h to complete the oxidation process. Subsequently, 30 mL of 30% H_2O_2 was slowly added to neutralize the excess $KMnO_4$ and terminate the reaction. The color of the solution changed to light brown, indicating the successful synthesis of graphite oxide (GrO).

The resulting suspension was filtered using a vacuum filtration system with a cellulose nitrate membrane to separate the solid graphite oxide from the acidic solution. The residue retained on the membrane was collected, thoroughly washed, and air-dried to obtain graphite oxide powder. To exfoliate the graphite oxide into GO, 1.0 g of graphite oxide was dispersed in 250 mL of deionized water and subjected to ultrasonication in a bath sonicator for 2 h. This process resulted in a stable GO dispersion, which was subsequently refiltered to remove any remaining unexfoliated particles or large agglomerates.

2.3 Functionalization of graphene oxide (f-GO)

Owing to the poor dispersibility of GO in non-polar media, surface functionalization was performed to enhance its compatibility with the PAO base oil. Sodium dodecyl sulfate (SDS) was employed as a surfactant to prevent agglomeration of graphene oxide (GO) nanosheets and to enhance their dispersion stability in the PAO base oil. SDS adsorption on GO surfaces improves interparticle repulsion and effectively retards aggregation (Zhang et al., 2019a; Thickett and Zetterlund, 2015; Hsieh et al., 2013). In this study, SDS (Merck) was used as the functionalizing agent, with ethanol as the solvent medium. A mass ratio of 1 g SDS per 100 mL ethanol was adopted to ensure sufficient surfactant availability and promote effective surface coverage of GO nanosheets, facilitating improved interfacial compatibility with the non-polar PAO environment.

The SDS–ethanol solution was first ultrasonicated for 30 min to ensure complete SDS dissolution. Then, 0.78 g of GO powder was added to the SDS–ethanol mixture to obtain a GO-to-solvent ratio of 1 wt%. This excess SDS condition was maintained to avoid surfactant deficiency during functionalization. The resulting mixture was ultrasonicated for 2 h, followed by continuous magnetic stirring for 12 h at a temperature of 60°C. The low-temperature constraint was imposed to prevent GO sheet agglomeration, which can occur at elevated temperatures due to ethanol evaporation and van der Waals attractions.

After the functionalization step, the mixture was filtered using Whatman filter paper No. 42 with a pore size of 2.5μm. The solid residue retained on the filter was then dried in a low-temperature oven at 50°C to allow gradual ethanol evaporation without inducing aggregation. This was feasible due to the low boiling point of ethanol (78°C), which permitted solvent removal at sub-boiling temperatures. The dried product was collected as functionalized graphene oxide and stored in a desiccator before incorporation into the lubricant matrix.

2.4 Characterization and tribological analysis

To confirm the successful oxidation of graphite to GO, the GO samples were subjected to a series of physicochemical characterizations. The synthesized GO was analyzed using the following techniques. Scanning Electron Microscopy with Energy-Dispersive X-ray Spectroscopy (SEM–EDS: This technique is used to observe morphological changes due to oxidation and to qualitatively assess the elemental composition, particularly the increase in oxygen content. Fourier transform infrared spectroscopy (FTIR), this technique is used to identify functional groups associated with oxygen-containing bonds (e.g., hydroxyl, epoxy, and carboxyl), indicating successful chemical modification. X-ray diffraction (XRD), XRD was used to analyze interlayer spacing changes and crystallinity, differentiating between the ordered structure of graphite and the more amorphous structure of GO. Ultraviolet–Visible Spectroscopy (UV–Vis): Performed to detect π–π^* and n–π^* transitions associated with C=C and C=O bonds, further confirming oxidation and partial delocalization of electronic states.

The tribological performance of the f-GO–PAO nanolubricants was evaluated using the High-Frequency Reciprocating Rig (HFRR) method, a widely accepted standard for boundary lubrication assessment. The test followed conditions adapted from ASTM D6079 and was used to measure the following parameters: Coefficient of friction (CoF): continuously recorded throughout the test duration. Wear track diameter (scar width): Measured on the steel ball using optical microscopy to assess material protection. Film formation characteristics: The lubricant's load-carrying and film-forming ability was evaluated based on frictional behavior and post-test surface observations. To ensure reproducibility and comparability across samples, all tests were conducted under consistent environmental and load conditions.

3. Results and Discussion

Figure 1 provides a schematic overview of the fabrication process of GO derived from battery waste, specifically for its application as a friction modifier in lubricants. The process began with the recovery of graphite rods from spent battery materials, which were then purified to remove residual contaminants. This purified graphite undergoes chemical oxidation—typically using a modified Hummers method—to introduce oxygen-containing functional groups, forming GO with an expanded interlayer structure. The synthesized GO is then dispersed into a base lubricant of PAO through mechanical stirring and ultrasonication to produce a homogeneous GO-lubricant formulation.

3.1 Graphene oxide analysis

After chemical oxidation, a series of characterizations were conducted to confirm that GO was successfully synthesized. Figure 2 shows the X-ray diffraction patterns of graphite and GO. The graphite recovered from dry cell battery waste, inset shows a prominent diffraction peak at $2\theta \approx 26.6°$, which corresponds to the (002) plane of crystalline graphite (Popova, 2017). Upon oxidation, a significant peak shift is observed at $2\theta \approx 11.07°$ in the GO sample, which is characteristic of the (001) plane of GO (Stobinski et al., 2014; Krishnamoorthy et al., 2013). This shift indicates the successful oxidation of graphite and the intercalation of oxygen-containing functional groups and water molecules between the graphene layers. Additionally, a secondary peak at $2\theta \approx 17.45°$, which may be attributed to intermediate oxidation states, partial restacking, or structural disorder within the GO layers (Gascho et al., 2019). Table 1 lists some XRD

parameters from graphite and GO, such as the d-spacing, crystallite size (t), and the number of layers of each crystallite (N).

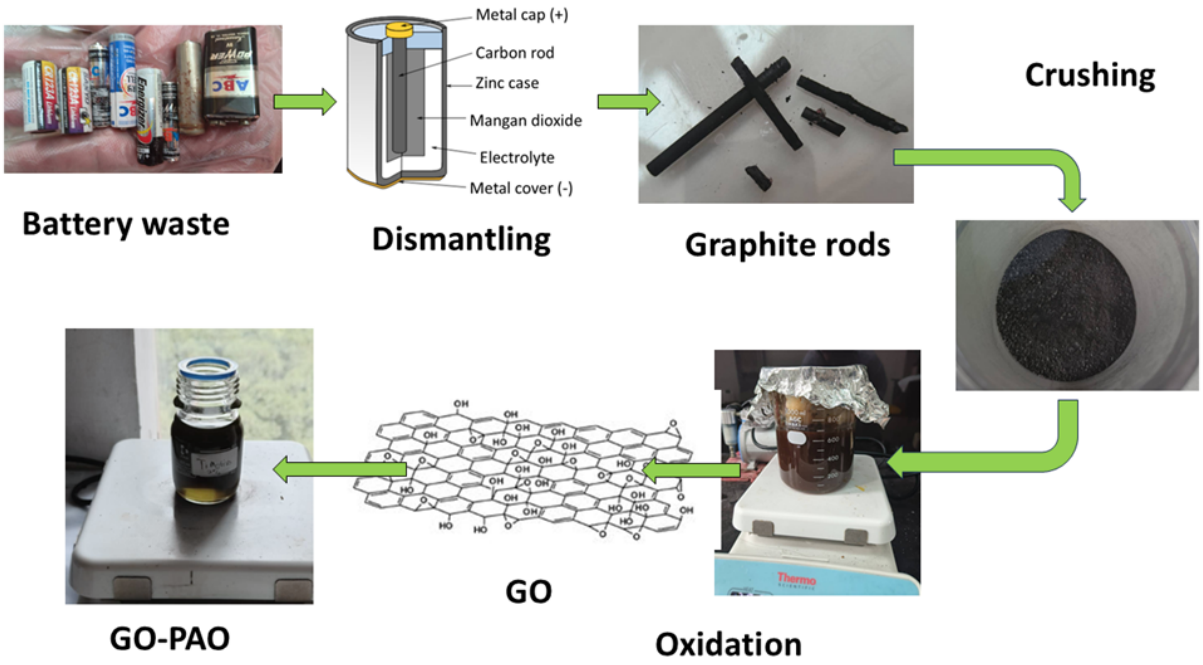

Figure 1 Schematic of the GO fabrication process as a friction modifier synthesized from battery waste. The process involves the extraction of graphite from spent battery materials, followed by chemical oxidation to produce GO, which is subsequently incorporated into base oil for tribological applications

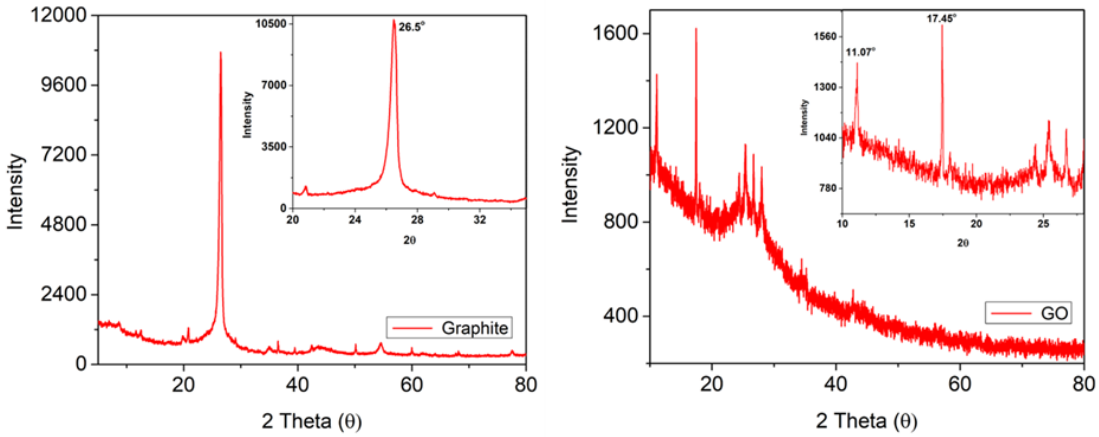

Figure 2 X-ray diffraction patterns of graphite (left) and GO (right). The inset highlights a strong diffraction peak at $2\theta \approx 26.5°$, which is characteristic of the crystalline graphite (002) plane, whereas the typical peak at $2\theta \approx 11.07°$, which is characteristic of the (001) plane of GO, indicates successful oxidation and interlayer spacing due to oxygen-containing functional groups. A secondary peak appears at $2\theta \approx 17.45°$, which may be attributed to partially oxidized regions or residual graphitic domains

Table 1 presents the XRD parameters for graphite and GO, highlighting the structural changes induced by the oxidation process. The pristine graphite sample shows a sharp diffraction peak at $2\theta = 26.6°$, which corresponds to an interlayer spacing (d) of 3.35 $\mathring{A}$, typical of the (002) plane in well-crystallized graphite. In contrast, the first prominent GO peak appears at $2\theta = 11.07°$, indicating a substantial increase in the interlayer spacing to 7.95 $\mathring{A}$. This expansion

is attributed to the successful intercalation of oxygen-containing functional groups and water molecules between the graphene layers during chemical oxidation. Secondary peak at $2\theta = 17.45°$ with a d-spacing of 5.07 $\AA$ shows the presence of partially oxidized or restacked GO structures.

Table 1 Summary of the XRD parameters of graphite and graphene oxide

Parameter	Graphite	1^{st} peak GO	2^{nd} peak GO
2θ (°)	26.6	11.07	17.45
d (Å)	3.35	7.95	5.07
t (nm)	155.77	92.86	120.25
N	465.90	116.81	237.31

The crystallite thickness (t), calculated using the Scherrer equation, decreases from 155.77 nm for graphite to 92.86 nm for the first GO peak, implying a reduction in stacking order due to oxidation. Interestingly, the second GO peak corresponds to a slightly larger crystallite size of 120.25 nm, possibly reflecting more ordered or less oxidized domains. The number of resulting layers (N value) can be calculated by dividing t by d. The estimated N-value decreased significantly from 465.90 in graphite to 116.81 in GO, confirming that oxidation exfoliates and disrupts the original graphitic stacking. This showed that exfoliation due to oxidation had occurred.

Figure 3 presents the SEM characterization of graphite (a and c) and graphene oxide (GO) (b and d) synthesized from dry cell battery waste. The graphite samples exhibited a morphology dominated by densely stacked flake-like structures, indicating tightly packed graphite layers. In contrast, the GO samples displayed a more delaminated morphology, characterized by sheet-like structures with fewer stacked layers and increased transparency. This transformation demonstrates that exfoliation occurred following the oxidation process. Such morphological evolution is consistent with previous reports, which describe that oxidative treatment introduces oxygen-containing functional groups (e.g., hydroxyl, epoxy, and carboxyl groups) into the graphite lattice, weakening interlayer van der Waals interactions and promoting layer separation (Chiang et al., 2023; Amir Faiz et al., 2020; Kusrini et al., 2019; Nasir et al., 2019). These morphological changes are consistent with the elemental composition obtained from EDS analysis (Table 2), which shows that GO contains 86% carbon and 11.25% oxygen, confirming the successful incorporation of oxygen functional groups during oxidation.

The UV–Vis absorption spectrum provides further evidence supporting the successful oxidation of graphite to GO, as shown in Figure 4. The spectrum displays a prominent peak at 233 nm, corresponding to the $\pi \rightarrow \pi^*$ transition of aromatic C=C bonds, and a shoulder around 298 nm, attributed to the n→π^* transition of C=O bonds, which has also been reported in many works (Thangavel et al., 2015; Lim et al., 2013; Rattana et al., 2012). These characteristic transitions indicate conjugated π-systems and oxygen-containing functional groups. Such spectral features confirm that the oxidation process altered the electronic structure of graphite, introducing oxygen functionalities and disrupting the sp^2-hybridized carbon framework, consistent with the formation of GO.

Figure 5 shows the FTIR spectra of GO. Several distinct peaks corresponding to oxygen-containing functional groups introduced during oxidation are observed. A broad peak at 3159 cm^{-1} corresponds to O–H stretching vibrations, indicating the presence of hydroxyl groups and possibly water molecules intercalated within the layered structure. The peak at 2807 cm^{-1} is attributed to C–H stretching. The sharp peak at 1709 cm^{-1} corresponds to C=O stretching, indicating carboxyl or carbonyl groups, whereas the peak at 1627 cm^{-1} is assigned to C=C skeletal vibrations of unoxidized sp^2 carbon domains. The peak at 1196 cm^{-1} is associated with C–O stretching, corresponding to the epoxy groups. Collectively, these functional groups confirm the successful oxidation and partial exfoliation of graphite. Moreover, the presence of

C=C and C=O bonds is consistent with the UV–Vis spectroscopy results, thereby reinforcing the structural and chemical transformation of graphite to GO.

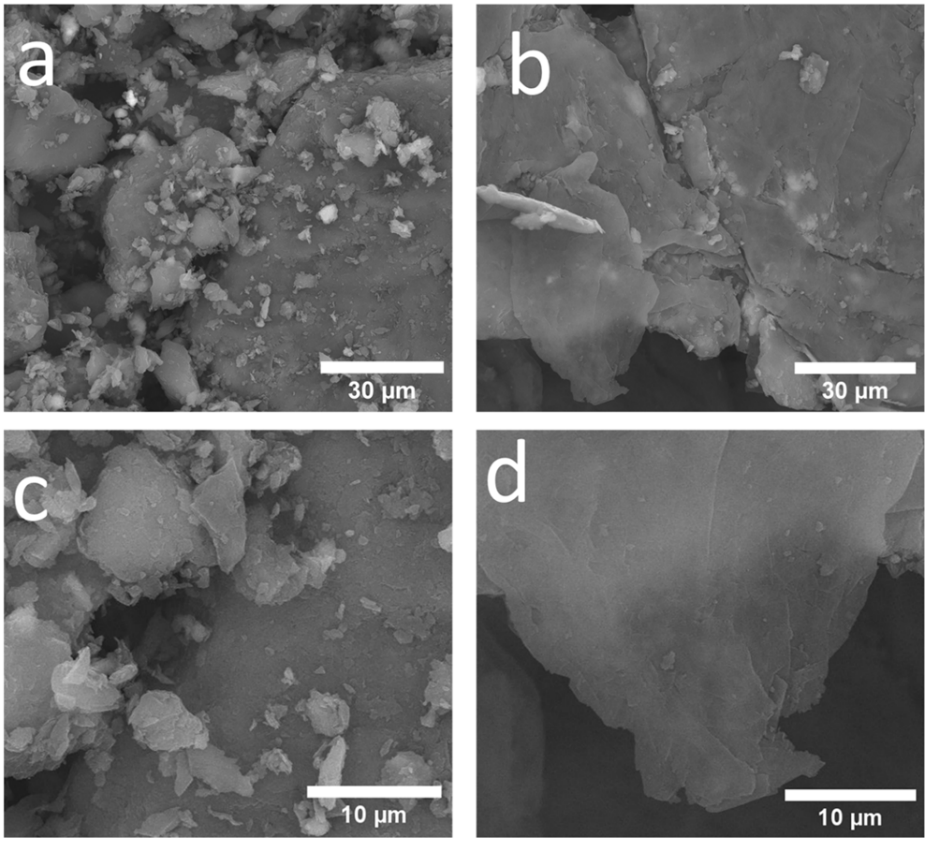

Figure 3 SEM images of (a and c) graphite and (b and d) GO at different magnifications. Graphite morphology predominantly comprises compact, stacked flakes, whereas graphene oxide (GO) exhibits thicker, more separated sheet-like structures. This morphological transition indicates the successful oxidation and exfoliation of graphite during the synthesis process, resulting in the expansion and delamination of layers in the GO structure

Table 2 Composition of GO synthesized from the carbon of battery waste

	C%	O%	Si%	Al%
GO	86%	11.25%	00.57%	00.49%

3.2 Tribological performance of the GO–PAO system

After a series of characterization techniques confirmed that the obtained carbon material was GO, the GO was incorporated into a polyalphaolefin (PAO) base oil as a friction-modifying additive. The tribological performance of the lubricant formulations was investigated using a High-Frequency Reciprocating Rig (HFRR) by the ASTM D6079 standard (ASTM International, 2024). Figure 6 shows a schematic representation of the HFRR setup. The HFRR test was conducted under the following conditions: the lubricant temperature was maintained at 60 °C, with a normal load of 2 N, a reciprocating frequency of 50 Hz, a stroke length of 1000 μm, and a lubricant volume of 2 mL. The testing configuration comprised two interacting specimens. The upper specimen was a steel ball made of AISI E-52100 bearing steel, with hardness 60–67 HRC (Rockwell C scale), whereas the lower specimen was a flat disc, also made of AISI E-52100 steel, machined from an annealed rod and exhibiting a Vickers hardness of approximately 30 HV. The upper steel ball underwent a reciprocating motion against the stationary lower disc,

which was partially submerged in the lubricant during the operation. The upper ball was the primary surface analyzed for friction coefficient and wear scar diameter, whereas the lower disc functioned as both the counterface and a lubricant reservoir.

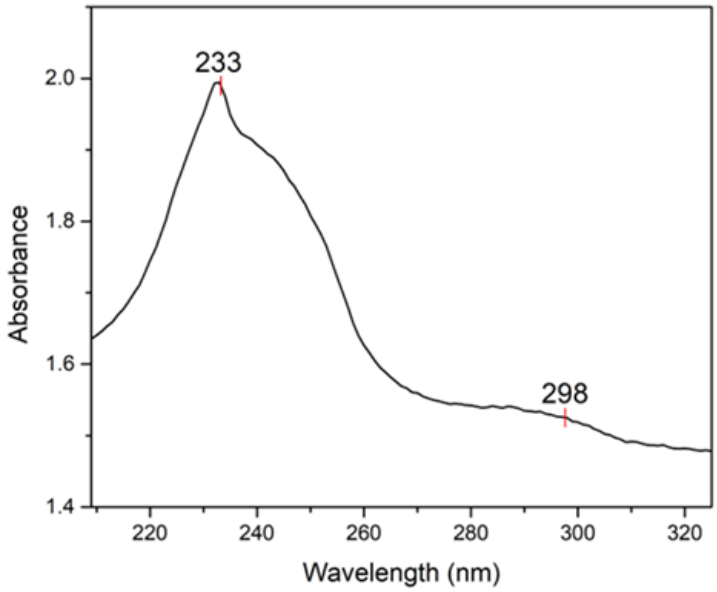

Figure 4 UV–Vis absorption spectrum of GO synthesized from dry cell battery waste. The spectrum exhibited a strong absorption peak at 233 nm, corresponding to the $\pi \rightarrow \pi^*$ transition of aromatic C=C bonds, and a shoulder at approximately 298 nm, attributed to the $n \rightarrow \pi^*$ transition of C=O functional groups. These features confirm the presence of conjugated structures and oxygen-containing groups, indicating successful GO oxidation

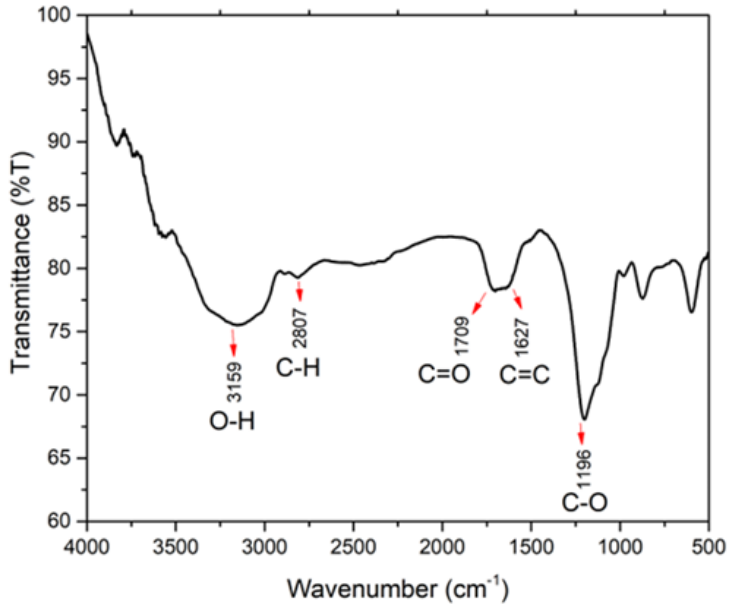

Figure 5 FTIR spectra of GO synthesized from dry cell battery waste. The spectrum reveals characteristic absorption bands indicating oxygen-containing functional groups, confirming the successful oxidation of GO

3.2.1 Coefficient of friction (CoF)

Figure 7 shows that incorporating GO into PAO significantly reduces the CoF. The pure PAO lubricant exhibited an average CoF of 0.148. When GO was added at concentrations of

1%, 3%, and 5%, the average CoF values decreased to 0.082, 0.129, and 0.131, respectively. These values correspond to a CoF reduction of approximately 44.6%, 12.8%, and 11.5%, respectively, compared to pure PAO. The 1% GO–PAO formulation significantly reduced friction. The addition of a higher concentration of GO will increase the CoF again, indicating that a lower concentration of GO may be more effective in forming a uniform tribofilm and enhancing lubricity under the given test conditions.

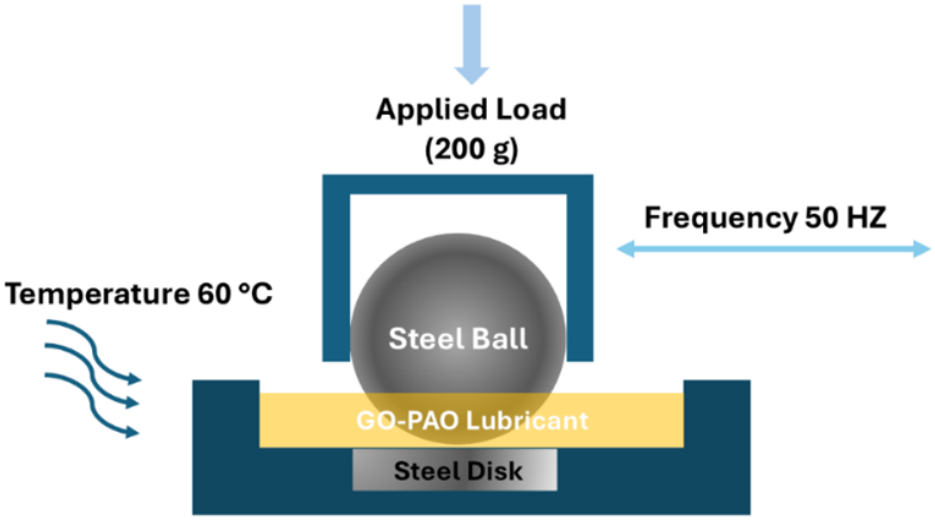

Figure 6 Schematic of the HFRR test apparatus used to investigate the tribological performance of the lubricant. The setup replicates sliding contact under controlled conditions, enabling the quantitative measurement of critical parameters, such as friction coefficient and wear scar diameter. This standardized test method provides insight into the lubricating effectiveness and anti-wear properties of the formulated samples

Furthermore, the CoF analysis over time revealed distinct fluctuation patterns across all lubricant formulations. The CoF exhibited notable variability for pure PAO, ranging from 0.120 to 0.178 throughout the testing duration, indicating limited film stability under dynamic loading. In contrast, the GO 1%–PAO blend exhibited a narrower fluctuation, ranging from 0.090 to 0.115 in the early phase of the test. Notably, after approximately 17 minutes, the CoF of this formulation exhibited a pronounced decrease to approximately 0.070 after approximately 17 min, after which it stabilized, indicating the formation of a robust and continuous tribofilm. The CoF of the GO 3%–PAO blend remained relatively stable, fluctuating between 0.110 and 0.147, whereas that of the GO 5%–PAO blend showed a similar trend, ranging between 0.114 and 0.147. These observations indicate that the addition of GO improves the stability of the lubricating film, particularly at low concentrations. GO 1% demonstrated superior performance in suppressing friction and enhancing long-term consistency under sliding conditions. Overall, the observed reduction in friction upon GO addition is in good agreement with earlier studies, which reported that graphene oxide nanosheets act as an additive in the lubricant system (Liu et al., 2019; Mungse and Khatri, 2014).

3.2.2 Tribofilm formation

The addition of GO enhances the film-forming stability and capability of the lubricant, as illustrated in Figure 8. The average film formation percentages observed for pure PAO, GO 1 wt%–PAO, GO 3 wt%–PAO, and GO 5 wt%–PAO were 87%, 95%, 99%, and 99%, respectively. These results indicate that GO improves the lubricant's ability to form a consistent tribofilm. However, the improvement plateaus beyond the 3 wt% loading, as the film formation percentage remains unchanged at 99% for both 3% and 5% GO concentrations. Furthermore, the temporal trend of film formation during the test shows that increasing the f-GO content

reduces fluctuations, demonstrating a more stable and continuous boundary lubrication regime. This behavior is attributed to the formation of a protective GO-based tribolayer that reduces asperity contact and enhances the load-carrying capacity under reciprocating motion.

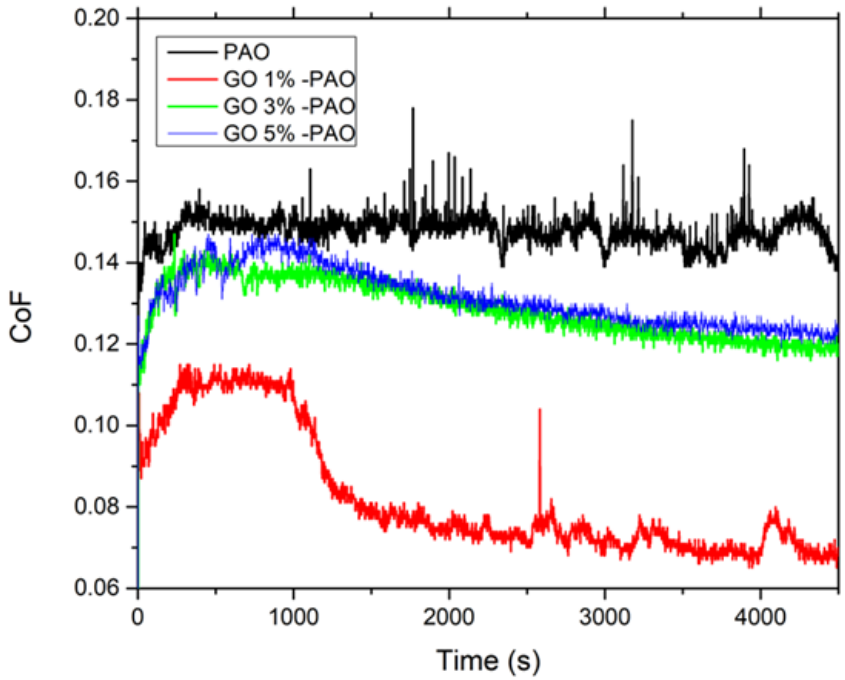

Figure 7 Coefficient of friction (CoF) results obtained from HFRR testing of PAO base oil and GO–PAO lubricants with varying GO concentrations (1 wt%, 3 wt%, and 5 wt%). The results demonstrate the influence of GO content on friction reduction under reciprocating sliding conditions over a 75-min test duration.

For pure PAO oil, the film formation exhibited noticeable fluctuations, ranging between 65% and 90% throughout the testing period, indicating limited stability in the boundary lubrication regime. In contrast, the GO 1 wt%–PAO formulation significantly improved the film formation behavior. Initially, film formation gradually increased from 35% to 95%, and after approximately 19 min, the value stabilized, maintaining a consistent range between 99% and 100% for the remainder of the test. This indicates the successful establishment of a robust and continuous tribolayer. The 3 wt% and 5 wt% GO–PAO blends exhibited similar behavior, with film formation fluctuating narrowly within the 95%–100% range and remaining largely stable throughout the test duration. These findings confirm that GO incorporation enhances the maximum film formation capability and temporal stability, particularly at 1 wt% and above.

A clear correlation was observed between film formation and CoF, particularly in the case of the GO 1 wt%–PAO formulation. As shown in the results, a noticeable reduction in CoF began around the 17-min mark, coinciding with a significant increase in film formation, which stabilized at 99%–100% by approximately 19 min. This temporal alignment confirms that the development of a stable lubricating film directly reduces friction by minimizing direct surface-to-surface contact. Furthermore, a consistent trend was evident across all GO–PAO samples: higher average film formation percentages are associated with lower average CoF values. Compared to pure PAO, which exhibited both lower film formation and higher friction, the GO-enriched formulations demonstrate superior tribological performance, confirming the role of GO in enhancing lubricating film stability and effectiveness. The present findings are consistent with previous reports demonstrating that a protective layered carbon tribofilm contributes to the inherent low shear strength, reducing the CoF (Samanta et al., 2024; Wen et al., 2020).

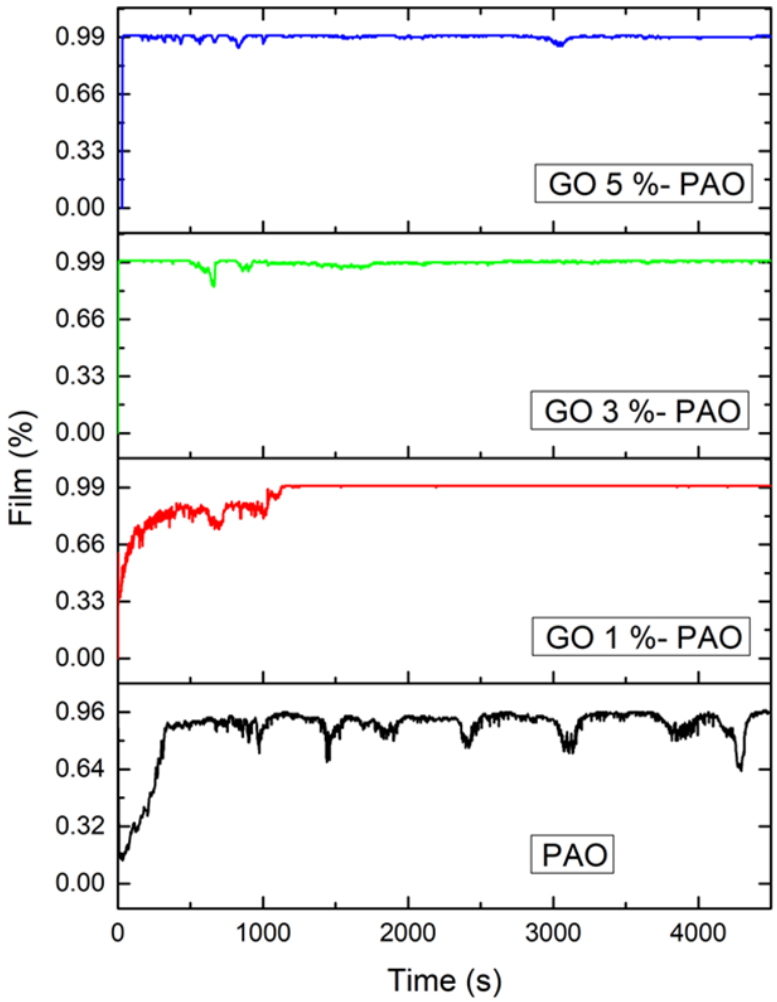

Figure 8 Tribofilm percentage results for three different concentrations of GO–PAO lubricant formulations (1 wt%, 3 wt%, and 5 wt% GO) compared to pure PAO as a reference. The data illustrate the influence of GO concentration on tribo-film stability and coverage over a 75-min sliding duration

3.2.3 Wear Analysis

Figure 9 (supplementary) shows the wear tracks and their corresponding widths. The measured WSD for pure PAO, GO 1wt%–PAO, GO 3wt%–PAO, and GO 5wt%–PAO were 432 μm, 201 μm, 145 μm, and 150 μm, respectively. These results indicate significant reductions in wear with the addition of GO. Specifically, the WSD decreased by 53.47% for the 1% formulation, 66.43% for the 3% formulation, and 65.27% for the 5% formulations, respectively, compared to pure PAO. All values are well below the ASTM D6079 standard limit of 520 μm for acceptable wear performance, confirming that the GO-enhanced lubricants not only comply with industrial standards but also exhibit superior antiwear properties. The formation of a protective tribolayer by GO, which minimizes direct metal-to-metal contact and enhances surface protection under reciprocating sliding conditions, is attributed to the substantial reduction in the size of the wear scar. The significant decrease in wear scar diameter after GO incorporation is in good agreement with earlier studies reporting that graphene oxide nanosheets improve antiwear behavior by forming a protective tribofilm and acting as a load-bearing layer at the sliding interface (Wang et al., 2019; Kinoshita et al., 2014).

Theoretically, the WSD in tribological testing is primarily influenced by the tribofilm percentage and CoF. Figure 10 (supplementary) shows that the PAO base oil sample exhibited a relatively high CoF of 0.148 and a corresponding large wear scar of 432 μm. In contrast, adding

1 wt% GO resulted in a substantial reduction in both CoF and WSD, with values dropping to 0.082 and 201 μm, respectively. This can be attributed to the formation of a stable GO tribo-film that acts as a protective barrier between the steel surfaces, effectively transitioning the contact mode from steel–steel to GO–GO, thereby reducing interfacial shear and adhesive wear.

Interestingly, further increases in GO concentration, as seen in the GO 3 wt%-PAO sample, produced a nonlinear trend: while the CoF increased slightly to 0.129, the WSD decreased significantly to 145 μm. A similar pattern was observed for the GO 5 wt%-PAO sample, which showed a CoF of 0.131 and a WSD of 150 μm. These observations indicate that the relationship between the CoF and WSD is not strictly proportional. The underlying mechanism can be explained as follows: the well-dispersed GO nanosheets quickly form a uniform, thin protective film that reduces both friction and wear at low GO concentration (1 wt%). However, with increasing GO content (3% and 5%), although the CoF increases slightly, the thicker deposition of GO results in a more robust antiwear layer, which continues to reduce the WSD (Wu et al., 2022; Tian et al., 2020; Zhang et al., 2019b). This effect is attributed to the increased quantity of GO available to fill surface asperities and maintain contact surface separation. However, this increased deposition also contributed to shear-induced interactions between each GO layer, which contributed to the slight increase in CoF. Nevertheless, the overall friction coefficient values for the 3% and 5% GO–PAO samples remained significantly lower than those of the PAO base oil, confirming the continued beneficial role of GO in lubrication. Thus, higher GO concentrations enhanced wear resistance by forming a thicker tribo-film that acts as a mechanical barrier rather than merely reducing friction. In summary, these findings reveal that friction reduction and antiwear performance do not always scale linearly with each other and that the optimal tribological behavior is governed by a balance between GO concentration, dispersion uniformity, and film-forming ability under sliding conditions.

4. Conclusions

Graphene oxide (GO) synthesized from graphite recovered from spent dry cell batteries has been demonstrated as a viable nano-additive for poly-alpha olefin (PAO). The recovered graphite exhibited a flake-like morphology and high carbon purity, confirming its suitability as a precursor. The successful oxidation via the modified Hummers method was verified through comprehensive characterization. SEM–EDS analysis revealed partial exfoliation and increased oxygen content, while XRD analysis confirmed the oxidation of graphite, as evidenced by the emergence of a characteristic GO diffraction peak at 2θ 11.07°°, corresponding to an expanded interlayer spacing from 3.35 $\mathring{A}$ to 7.95 $\mathring{A}$. FTIR spectroscopy identified hydroxyl, carboxyl, and epoxy functional groups, and UV–Vis spectra displayed absorption peaks at 233 and 298 nm, consistent with $\pi \rightarrow \pi^*$ (C=C) and n$\rightarrow\rightarrow \pi^*$ (C=O) transitions. The tribological evaluation using HFRR demonstrated a concentration-dependent and nonlinear relationship between friction and wear behavior. The 1 wt% GO–PAO formulation exhibited the lowest coefficient of friction, achieving approximately 45% reduction relative to neat PAO, along with significant wear reduction and improved film stability. In contrast, the minimum wear scar diameter was obtained at 3 wt% GO, indicating enhanced load-bearing capacity associated with the formation of a thicker or more compact protective tribolayer. Increasing the concentration to 5 wt% did not provide additional benefit, indicating that excessive loading may promote nanosheet aggregation and reduce dispersion efficiency. Overall, 1 wt% GO demonstrated the most pronounced friction-reducing performance, whereas moderate concentrations primarily enhanced wear resistance, revealing a concentration-dependent friction–wear trade-off governed by tribofilm evolution. The nonlinear behavior observed across formulations underscores the importance of optimizing additive loading to balance shear stress reduction and load-bearing capacity in boundary lubrication regimes. This study establishes a technically viable pathway for converting battery waste–derived graphite into high-value graphene oxide nano-additives.

Acknowledgements

The authors gratefully acknowledge the financial support for the Article Processing Charge (APC) provided by the Unit of Research, Innovation, and Community Engagement, Faculty of Engineering, Universitas Indonesia under contract no NKB-1043/UN2.F4.D/PPM.00.04/2026". The authors gratefully acknowledge the support of the Research Center for Oil and Gas Technology Development for their facilities and technical assistance throughout this study.

Author Contributions

Alfian Ferdiansyah: Conceptualization, Recourses, Data Curation, Formal Analysis, Validation, Visualization, Original Draft Writing, Review, and Editing. Muhammad Ibadurrohman: Data curation and review. Timotius Tanusondjaja, Cahyo Setyo Wibowo, and Riesta Anggarani: Methodology and Investigation Havid Aqoma: Formal analysis, review, and editing.

Conflict of Interest

The authors declare no conflicts of interest.

References

Abdelbary, A., & Chang, L. (2023a). Lubricants and their properties [Chapter 8]. In *Principles of engineering tribology*. Academic Press.

Abdelbary, A., & Chang, L. (2023b). Practical applications of tribology [Chapter 10]. In *Principles of engineering tribology*. Academic Press.

Amir Faiz, M. S., Che Azurahanim, C. A., Raba'ah, S. A., & Ruzniza, M. Z. (2020). Low-cost and green reduction of graphene oxide (GO) using palm oil leaves extract for industrial applications. *Results in Physics*, *16*, 102954. https://doi.org/10.1016/j.rinp.2020.102954

Amiri, M., & Khonsari, M. M. (2010). On the Thermodynamics of friction and wear: A review. *Entropy*, *12*(5), 1021–1049.

ASTM International. (2024). *Standard test method for evaluating lubricity of diesel fuels by the high-frequency reciprocating rig (HFRR)* (tech. rep.) (ASTM Volume 05.02). ASTM International. Pennsylvania, United States.

Bowden, F. P., Leben, L., & Taylor, G. I. (1997). The friction of lubricated metals. *Philosophical Transactions of the Royal Society A*, *239*, 1–27. https://doi.org/10.1098/rsta.1940.0007

Brinksmeier, E., Meyer, D., Huesmann-Cordes, A. G., & Herrmann, C. (2015). Metalworking fluids: Mechanisms and performance. *CIRP Annals*, *64*, 605–628. https://doi.org/10.1016/j.cirp.2015.05.003

Chiang, A. K. M., Ng, L. Y., Ng, C. Y., Lim, Y. P., Mahmoudi, E., Tan, L. S., & Mah, S. K. (2023). Conversion of palm oil empty fruit bunches to fluorescent graphene oxide quantum dots: An eco-friendly approach. *Materials Chemistry and Physics*, *309*, 128433. https://doi.org/10.1016/j.matchemphys.2023.128433

Dai, Y., Feng, X., Liu, Y., Huang, J., Wu, S., Zhou, P., & Li, H. (2024). Onion-like carbon nanoparticles as lubricant additives for improved tribological performance. *Materials Chemistry and Physics*, *314*, 128836. https://doi.org/10.1016/j.matchemphys.2023.128836

Dreyer, D. R., Park, S., Bielawski, C. W., & Ruoff, R. S. (2010). Chemistry of graphene oxide. *Chemical Society Reviews*, *39*, 228–240. https://doi.org/10.1039/B917103G

Erdemir, A., & Donnet, C. (2001). Solid lubricants and self-lubricating films. In *Handbook of modern tribology* (pp. 787–818).

Gascho, J. L. S., Costa, S. F., Recco, A. A. C., & Pezzin, S. H. (2019). Graphene oxide films obtained by vacuum filtration: X-ray diffraction evidence of crystalline reorganization. *Journal of Nanomaterials*, *2019*, 5963148. https://doi.org/10.1155/2019/5963148

Gasni, D., Mulyadi, I. H., Affi, J., & Miswar, A. Y. (2017). Investigation of wear mechanisms in ball bearings lubricated by bio-lubricants. *International Journal of Technology*, *8*(7), 1248–1257. https://doi.org/10.14716/ijtech.v8i7.688

Holmberg, K., Andersson, P., & Erdemir, A. (2012). Global energy consumption due to friction in passenger cars. *Tribology International*, *47*, 221–234. https://doi.org/10.1016/j.triboint.2011.11.022

Hsieh, A. G., Korkut, S., Punckt, C., & Aksay, I. A. (2013). Dispersion stability of functionalized graphene in aqueous sodium dodecyl sulfate solutions. *Langmuir*, *29*, 14831–14838. https://doi.org/10.1021/la4035326

Hummers, W. S., & Offeman, R. E. (1958). Preparation of graphitic oxide. *Journal of the American Chemical Society*, *80*, 1339–1339.

Kato, K. (2000). Wear in relation to friction: A review. *Wear*, *241*, 151–157. https://doi.org/10.1016/S0043-1648(00)00382-3

Kimura, R., Ferré-Pujol, P., & Nishina, Y. (2025). Grafting-through functionalization of graphene oxide with cationic polymers for enhanced adsorption. *Carbon*, *238*, 120296. https://doi.org/10.1016/j.carbon.2025.120296

Kinoshita, H., Kondo, M., Nishina, Y., & Fujii, M. (2015). Anti-wear effect of graphene oxide in lubrication by ionic liquids. *Tribology Online*, *10*, 91–95. https://doi.org/10.2474/trol.10.91

Kinoshita, H., Nishina, Y., Alias, A. A., & Fujii, M. (2014). Tribological properties of graphene oxide sheets as water-based lubricant additives. *Carbon*, *66*, 720–723. https://doi.org/10.1299/mej.15-00323

Kozlov, S., Viñes, F., & Görling, A. (2012). Bonding mechanisms of graphene on metal surfaces. *The Journal of Physical Chemistry C*, *116*, 7360–7366. https://doi.org/10.1021/jp210667f

Krishnamoorthy, K., Veerapandian, M., Yun, K., & Kim, S. J. (2013). The chemical and structural analysis of graphene oxide with different degrees of oxidation. *Carbon*, *53*, 38–49. https://doi.org/10.1016/j.carbon.2012.10.013

Kusrini, E., Suhrowati, A., Usman, A., Degirmenci, D. V., & Khalil, M. (2019). Synthesis and characterization of graphite oxide, graphene oxide, and reduced graphene oxide using modified Hummers method. *International Journal of Technology*, *10*, 1093–1104. https://doi.org/10.14716/ijtech.v10i6.3639

Li, B., Li, P., Zhou, R., Feng, X.-Q., & Zhou, K. (2022). Contact mechanics in tribological and contact damage-related problems: A review. *Tribology International*, *171*, 107534. https://doi.org/10.1016/j.triboint.2022.107534

Lim, S. P., Huang, N. M., & Lim, H. N. (2013). Solvothermal synthesis of SnO_2/graphene nanocomposites for supercapacitor applications. *Ceramics International*, *39*, 6647–6655. https://doi.org/10.1016/j.ceramint.2013.01.102

Liu, Y., Chen, X., Li, J., & Luo, J. (2019). Enhanced friction performance via synergistic effects of graphene oxide and molybdenum disulfide. *Carbon*, *154*, 266–276. https://doi.org/10.1016/j.carbon.2019.08.009

Liu, Y., Wang, X., Pan, G., & Luo, J. (2013). Comparative study of graphene oxide and diamond nanoparticles as water-based lubricant additives. *Science China Technological Sciences*, *56*, 152–157. https://doi.org/10.1007/s11431-012-5026-z

Mungse, H. P., & Khatri, O. P. (2014). Chemically functionalized reduced graphene oxide for reduction of friction and wear. *Journal of Physical Chemistry C*, *118*, 14394–14402. https://doi.org/10.1021/jp5033614

Nasir, S., Hussein, M. Z., Zainal, Z., & Yusof, N. A. (2019). Development of new carbon-based electrode material from oil palm waste-derived reduced graphene oxide and its capacitive performance evaluation. *Journal of Nanomaterials*, *2019*, 1970365. https://doi.org/10.1155/2019/1970365

Nyholm, N., & Espallargas, N. (2023). Functionalized carbon nanostructures as lubricant additives: A review. *Carbon*, *201*, 1200–1228. https://doi.org/10.1016/j.carbon.2022.10.035

Opia, A. C., Abdollah, M. F. B., Syahrullail, S., Amiruddin, H., Mamah, C. S., & Veza, I. (2025). Effectiveness of carbon nanomaterials as lubricant additives: Recent review. *Materials Today Nano*, *30*, 100643. https://doi.org/10.1016/j.mtnano.2025.100643

Paredes, J. I., Villar-Rodil, S., Martínez-Alonso, A., & Tascón, J. M. D. (2008). Graphene oxide dispersions in organic solvents. *Langmuir*, *24*, 10560–10564. https://doi.org/10.1021/la801744a

Pavani, P. N. L., Rao, R. P., & Prasad, C. L. V. R. S. V. (2017). Synthesis and experimental investigation of tribological performance of a blended (palm and mahua) bio-lubricant using the Taguchi design of experiment (DOE). *International Journal of Technology*, *8*(3), 418–427. https://doi.org/10.14716/ijtech.v8i3.6386

Perreault, F., Fonseca de Faria, A., & Elimelech, M. (2015). Environmental applications of graphene-based nanomaterials. *Chemical Society Reviews*, *44*, 5861–5896. https://doi.org/10.1039/C5CS00021A

Popova, A. N. (2017). Crystallographic analysis of graphite using X-ray diffraction. *Coke and Chemistry*, *60*, 361–365. https://doi.org/10.3103/S1068364X17090058

Rattana, Chaiyakun, S., Witit-Anun, N., Nuntawong, N., Chindaudom, P., Oaew, S., Kedkeaw, C., & Limsuwan, P. (2012). Preparation and characterization of graphene oxide nanosheets. *Procedia Engineering*, *32*, 759–764. https://doi.org/10.1016/j.proeng.2012.02.009

Samanta, S., Yoon, D.-H., & Sahoo, R. R. (2024). Covalently modified graphene oxide polymer brushes as efficient aqueous lubricant additives. *Journal of Molecular Liquids*, *416*, 126505. https://doi.org/10.1016/j.molliq.2024.126505

Son, S.-R., An, J., Choi, J.-W., Kim, S., Park, J., & Lee, J. H. (2021). Surface-anchored alkylated graphene oxide for liquid crystal alignment. *Materials Today Communications*, *28*, 102539. https://doi.org/10.1016/j.mtcomm.2021.102539

Stobinski, L., Lesiak, B., Malolepszy, A., Mazurkiewicz, M., Mierzwa, B., Zemek, J., Jiricek, P., & Bieloshapka, I. (2014). Graphene oxide and reduced graphene oxide studied by XRD, TEM, and spectroscopy. *Journal of Electron Spectroscopy and Related Phenomena*, *195*, 145–154. https://doi.org/10.1016/j.elspec.2014.07.003

Thangavel, S., Raghavan, N., Kadarkarai, G., Kim, S.-J., & Venugopal, G. (2015). Graphene oxide (GO)–Fe^{3+} hybrid nanosheets for sonocatalytic degradation. *Ultrasonics Sonochemistry*, *24*, 123–131. https://doi.org/10.1016/j.ultsonch.2014.11.019

Thickett, S. C., & Zetterlund, P. B. (2015). Graphene oxide nanosheets as oil-in-water emulsion stabilizers. *Journal of Colloid and Interface Science*, *442*, 67–74. https://doi.org/10.1016/j.jcis.2014.11.047

Tian, S., Gao, K., Zhang, H., Cui, H., & Zhang, G. (2020). Corrosion resistance and anti-wear properties of Ni–W–GO nanocomposite coatings. *Transactions of the Indian Institute of Metals*, *73*, 713–724. https://doi.org/10.1007/s12666-020-01864-5

Wang, R., Zhang, F., Yang, K., Xiao, N., Tang, J., Xiong, Y., Zhang, G., Duan, M., & Chen, H. (2024). Carbon materials in tribology: From lubrication mechanisms to wear behavior. *Journal of Alloys and Compounds*, *979*, 173454. https://doi.org/10.1016/j.jallcom.2024.173454

Wang, W., Zhang, G., & Xie, G. (2019). Ultralow concentration graphene oxide nanosheets as oil-based lubricant additives. *Applied Surface Science*, *498*, 143683. https://doi.org/10.1016/j.apsusc.2019.143683

Wen, P., Lei, Y., Li, W., & Fan, M. (2020). Two-dimensional layered nanomaterials as lubricant additives beyond graphene oxide. *Tribology International*, *143*, 106051. https://doi.org/10.1016/j.triboint.2019.106051

Wong, V. W., & Tung, S. C. (2016). Overview of automotive engine friction and reduction trends. *Friction*, *4*, 1–28. https://doi.org/10.1007/s40544-016-0107-9

Wu, D., Su, Q., Chen, L., Cui, H., Zhao, Z., Wu, Y., Zhou, H., & Chen, J. (2022). Achieving high anti-wear and corrosion protection of phenoxy-resin coatings reinforced with graphene oxide. *Applied Surface Science*, *601*, 154156. https://doi.org/10.1016/j.apsusc.2022.154156

Zaaba, N. I., Foo, K. L., Hashim, U., Tan, S. J., Liu, W.-W., & Voon, C. H. (2017). Synthesis of graphene oxide using modified Hummers method: Solvent influence. *Procedia Engineering*, *184*, 469–477. https://doi.org/10.1016/j.proeng.2017.04.118

Zapata-Hernandez, C., Geraldine, D.-G., Diana, L., Robison, B.-S., & Cacua, K. (2022). Improving stability of graphene nanofluids: Surfactants versus surface functionalization. *Journal of Dispersion Science and Technology*, *43*, 1717–1724.

Zhang, F., Li, S., Zhang, Q., Liu, J., Zeng, S., Liu, M., & Sun, D. (2019a). Adsorption of surfactants on graphene oxide. *Journal of Molecular Liquids*, *276*, 338–346. https://doi.org/10.1016/j.molliq.2018.12.009

Zhang, Y., Chen, F., Zhang, Y., Liu, Z., Wang, X., & Du, C. (2019b). Influence of graphene oxide on antiwear and antifriction performance of MAO coatings. *Surface and Coatings Technology*, *364*, 144–156. https://doi.org/10.1016/j.surfcoat.2019.01.103